Title
Evidence for direct molecular oxygen production in CO2 photodissociation

Journal
Science, 346(6205)

ISSN
0036-8075

Authors
Lu, Zhou
Chang, Yih Chung
Yin, Qing-Zhu
et al.

Publication Date
2014-10-03

DOI
10.1126/science.1257156

Peer reviewed

Evidence for direct molecular oxygen production in CO_2 photodissociation
Zhou Lu *et al.*
Science **346**, 61 (2014);
DOI: 10.1126/science.1257156

33. A. Chitnis, D. Rawls, J. Moore, *AIDS Res. Hum. Retroviruses* **16**, 5–8 (2000).
34. J. Pépin, *Sex. Transm. Infect.* **88**, 307–312 (2012).
35. D. Vangroenweghe, *Philos. Trans. R. Soc. London Ser. B* **356**, 923–925 (2001).
36. J. D. de Sousa, C. Alvarez, A. M. Vandamme, V. Müller, *Viruses* **4**, 1950–1983 (2012).
37. P. M. Sharp, B. H. Hahn, *Nature* **455**, 605–606 (2008).
38. A. Huybrechts, *Transports et Structures de Development au Congo: Etude du Progres Economique de 1900-1970* (Mouton, Paris, 1970).
39. R. R. Gray *et al.*, *AIDS* **23**, F9–F17 (2009).
40. J. Flouriot, *Introduction a la Geographique Physique et Humaine du Zaire* (Lyon, France, 1994, mimeographed).
41. W. A. Hance, *Population, Migration, and Urbanization in Africa* (Columbia Univ. Press, New York, 1970).
42. T. C. Quinn, *Proc. Natl. Acad. Sci. U.S.A.* **91**, 2407–2414 (1994).
43. M. Ngimbi, *Kinshasa, 1881–1981: 100 Ans Après Stanley: Problèmes et Avenir d'une Ville* (Ed Centre de Recherches Pédagogiques, Kinshasa, 1982).
44. P. Lemey, A. Rambaut, O. G. Pybus, *AIDS Rev.* **8**, 125–140 (2006).
45. C. Mulanga-Kabeya *et al.*, *AIDS* **12**, 905–910 (1998).
46. N. Nzilambi *et al.*, *N. Engl. J. Med.* **318**, 276–279 (1988).
47. S. M. Duke-Sylvester, R. Biek, L. A. Real, *Philos. Trans. R. Soc. London Ser. B* **368**, 20120194 (2013).
48. G. Magiorkinis *et al.*, *PLOS Comput. Biol.* **9**, e1002876 (2013).
49. J. C. Iles *et al.*, *Infect. Genet. Evol.* **19**, 386–394 (2013).
50. P. Beheyt, *Ann. Soc. Belg. Med. Trop.* **33**, 297–340 (1953).
51. J. D. de Sousa, V. Müller, P. Lemey, A. M. Vandamme, *PLOS ONE* **5**, e9936 (2010).
52. M. T. Gilbert *et al.*, *Proc. Natl. Acad. Sci. U.S.A.* **104**, 18566–18570 (2007).
53. J. Hemelaar, E. Gouws, P. D. Ghys, S. Osmanov; WHO-UNAIDS Network for HIV Isolation and Characterisation, *AIDS* **25**, 679–689 (2011).
54. C. Kuyu, *Les Haitiens au Congo* (L'Harmattan, Paris, 2006).
55. Institut National de la Statistique, *Étude Socio-Demographique de Kinshasa, 1967: Rapport General* (Institut National de la Statistique, Kinshasa, 1969).
56. G. Bonacci, "Kuyu, Camille. – Les Haïtiens au Congo," in *Cahiers d'Etudes Africaines* (L'Harmattan, Paris, 2008), vol. 192, p. 895.
57. K. Jochelson, M. Mothibeli, J. P. Leger, *Int. J. Health Serv.* **21**, 157–173 (1991).
58. M. H. Schierup, R. Forsberg, in *Proceedings of the Conference: Origins of HIV and Emerging Persistent Viruses*, 28 to 29 September 2001 (Accademia Nazionale dei Lincei, Rome, 2003), vol. 187, pp. 231–245.
59. M. H. Schierup, J. Hein, *Genetics* **156**, 879–891 (2000).
60. R. A. Neher, T. Leitner, *PLOS Comput. Biol.* **6**, e1000660 (2010).
61. M. J. Ward, S. J. Lycett, M. L. Kalish, A. Rambaut, A. J. Leigh Brown, *J. Virol.* **87**, 1967–1973 (2013).
62. P. Lemey *et al.*, *Genetics* **167**, 1059–1068 (2004).
63. J. O. Wertheim, M. Fourment, S. L. Kosakovsky Pond, *Mol. Biol. Evol.* **29**, 451–456 (2012).
64. L. de Saint-Moulin, *Villes et Organisation de l'Espace en République Démocratique du Congo* (L'Harmattan, Paris, 2010).

ACKNOWLEDGMENTS

We thank the researchers whose publicly available data made this work possible and A. M. Vandamme, M. L. Kalish, M. Worobey, and G. Leonard for helpful discussions. The research leading to these results has received funding from the European Union Seventh Framework Programme for research, technological development, and demonstration under grant agreement no. 278433-PREDEMICS and European Research Council grant agreement no. 260864. P.L. was partly supported by the "Onderzoeksfonds KU Leuven/Research Fund KU Leuven." M.A.S. is partly supported by NSF grant DMS 1264153 and NIH grant R01 HG006139. Collaboration between M.A.S., A.R., and P.L. was supported by the National Evolutionary Synthesis Center (NESCent) and NSF grant EF-0423641. This work was supported by the Wellcome Trust (grant 092807) to A.R. T.B. was supported by the Royal Society. J.D.S. is partly supported by the Fonds voor Wetenschappelijk Onderzoek Flanders grant G.0692.14. The data reported in this paper are deposited in the Dryad Repository (http://dx.doi.org/10.5061/dryad.nn952). Author contributions: P.L., O.G.P., A.R., M.A.S., M.P., and N.R.F. conceived the experiments and designed the study. N.R.F. and P.L. conducted the phylodynamic analyses. D.P. performed the recombination analysis and G.B. the model selection analysis. M.A.S. and T.B. contributed methodology. T.B., M.J.W., and N.A. assisted the sequence analysis. J.P., A.J.T., and J.D.S. contributed historical and spatial data. M.P. provided sequence data. N.R.F., P.L., O.G.P., and A.R. wrote the paper. All authors discussed the results and approved the final manuscript. We declare no competing financial interests.

SUPPLEMENTARY MATERIALS

www.sciencemag.org/content/346/6205/56/suppl/DC1
Materials and Methods
Figs. S1 to S9
Tables S1 to S9
References (*65–98*)

30 May 2014; accepted 3 September 2014
10.1126/science.1256739

REPORTS

PHOTOCHEMISTRY

Evidence for direct molecular oxygen production in CO_2 photodissociation

Zhou Lu,[1] Yih Chung Chang,[1] Qing-Zhu Yin,[2] C. Y. Ng,[1]* William M. Jackson[1]*

Photodissociation of carbon dioxide (CO_2) has long been assumed to proceed exclusively to carbon monoxide (CO) and oxygen atom (O) primary products. However, recent theoretical calculations suggested that an exit channel to produce C + O_2 should also be energetically accessible. Here we report the direct experimental evidence for the C + O_2 channel in CO_2 photodissociation near the energetic threshold of the $C(^3P) + O_2(X^3\Sigma_g^-)$ channel with a yield of 5 ± 2% using vacuum ultraviolet laser pump-probe spectroscopy and velocity-map imaging detection of the $C(^3P_J)$ product between 101.5 and 107.2 nanometers. Our results may have implications for nonbiological oxygen production in CO_2-heavy atmospheres.

It is widely accepted that the rise of the oxygen-rich atmosphere on Earth, known as the "Great Oxidation Event," occurred at ~2.4 billion years ago via multistep photosynthetic processes (Eq. 1) (*1*, *2*)

$$CO_2 + H_2O + h\nu \rightarrow (CH_2O) + O_2 \quad (1)$$

Here, h is Planck's constant and ν is the frequency. Over the past 40 years, biologists and paleontologists have proposed that free oxygen molecules must have been available in small quantities before the rise of oxygenic photosynthesis in Earth's prebiotic primitive atmosphere (*3*). The only known abiotic production mechanism was through solar vacuum ultraviolet (VUV) photodissociation of CO_2 to form CO + O in the early Earth stratosphere, followed by the three-body recombination reactions shown in Eqs. 2 and 3

$$CO_2 + h\nu(VUV) \rightarrow CO + O \quad (2)$$

$$O + O + M \rightarrow O_2 + M \quad (3)$$

Here, M is a third body for carrying off the excess energy involved in the formation of the O_2 chemical bond (*4*–*6*). Decades of experimental and theoretical photochemical studies of CO_2 have been focused on the detection and understanding of the CO + O photoproduct channels.

Recent theoretical calculations (*7*, *8*) suggest that an exit channel to produce C + O_2 upon VUV photoexcitation of the CO_2 molecule is possible. The ab initio calculation (*7*) has provided the dissociation pathway on the ground-state singlet potential energy surface of CO_2, leading to the formation of the $C(^3P) + O_2(X^3\Sigma_g^-)$ products (where X is indicative of the ground state) (pathway 1 of Fig. 1). If the electronically excited singlet CO_2 molecule initially produced by photoexcitation undergoes internal conversion to the ground-state singlet potential surface, the O atom could migrate through a cyclic CO_2 complex [c-$CO_2(^1A_1)$] and form a colinear $COO(^1\Sigma^+)$ intermediate before dissociation to $C(^3P) + O_2(X^3\Sigma_g^-)$, as shown in pathway 1. The theoretical calculation (*7*) predicts no potential energy barrier for this dissociation pathway. Grebenshchikov (*8*) calculated the singlet ground and excited potential energy surfaces of COO, with the O-O bond distance fixed at 2.3 bohr. His calculations indicate that the singlet ground and excited surfaces are connected by conical intersections, and his results support Hwang and Mebel's conclusion (*7*) that there is no potential energy barrier via the COO colinear state to yield $C(^3P) + O_2(X^3\Sigma_g^-)$ on the ground-state singlet surface. Despite these theoretical results, to our knowledge there has been no experimental verification of the C + O_2 channel in CO_2 photodissociation. Here we present the experimental evidence of $C(^3P) + O_2(X^3\Sigma_g^-)$

[1]Department of Chemistry, University of California, Davis, CA 95616, USA. [2]Department of Earth and Planetary Sciences, University of California, Davis, CA 95616, USA.
***Corresponding author. E-mail: cyng@ucdavis.edu (C.Y.N.); wmjackson@ucdavis.edu (W.M.J.)**

products based on VUV-pump and VUV-probe velocity-map imaging (VMI) measurements of $C(^3P_2)$ atoms. Direct detection of $O_2(X^3\Sigma_g^-)$ photoproducts is not feasible, in part due to the substantial number of O_2^+ background ions produced by photoionization of ambient O_2 molecules in the experimental chamber. Furthermore, state-selected VUV photoionization of $O_2(X^3\Sigma_g^-)$ photofragments would result in a much lower signal intensity compared with that of $C(^3P_J)$ atoms because a small fraction of $O_2(X^3\Sigma_g^-)$ products at a single rovibrational state is detected among the nascent $O_2(X^3\Sigma_g^-)$ produced in a wide range of rovibrational states, whereas the $C(^3P_J)$ atoms are only formed in three spin-orbit states.

In this CO_2 photodissociation experiment, the VUV photoexcitation energy $h\nu$(VUV) is distributed between the $C(^3P_J)$ and $O_2(X^3\Sigma_g^-)$ product translational energy (E_{trans}) and internal energy (E_{int}), where $E_{int}[C(^3P_J)]$ is due to excitation of the spin-orbit state; and the correlated $O_2(X^3\Sigma_g^-)$ photoproducts can be both rotationally and vibrationally excited. The VMI technique can be used to determine the recoil velocity distribution of the $C(^3P_J)$ photofragments from the radii of the resolved ring structures in the velocity-map image. The velocities are converted to a total kinetic energy release (TKER) spectrum of the $C(^3P_J) + O_2(X^3\Sigma_g^-)$ channel by using Eq. 4 based on the conservation of linear momentum and energy

$$h\nu(\text{VUV}) = D_0 + E_{int}[C(^3P_J)] + E_{int}[O_2(X^3\Sigma_g^-)] + E_{trans}[C(^3P_J) + O_2(X^3\Sigma_g^-)] \quad (4)$$

Here, D_0 = 11.44 eV is the thermochemical threshold for the formation of the $C(^3P_J) + O_2(X^3\Sigma_g^-)$ products from CO_2 dissociation (*7*). Equation 4 can also be used to determine the internal rotational and vibrational energy populations of $O_2(X^3\Sigma_g^-)$ photofragments from the TKER spectrum.

In the present experiment, a skimmed and pulsed supersonic molecular beam generated from ~10% CO_2 seeded in He was irradiated by two counter-propagating unfocused VUV laser beams, hereafter designated as "VUV_1" and "VUV_2" (*9*, *10*). The VUV_1 laser output was used to directly excite CO_2 to a dissociative rovibronic state. $C(^3P_J)$ photofragments were then selectively ionized via a VUV_2-visible (1+1′) resonance-enhanced photoionization scheme, which has been shown to achieve substantially higher detection sensitivities for $C(^3P_J)$ detection compared with those observed using a direct VUV photoionization method (*9*).

The ion species formed by photoionization in the interaction region were accelerated by the ion imaging optics into a time-of-flight (TOF) spectrometer for mass analyses and detected by a dual microchannel plates detector. Figure 2 depicts three TOF spectra in the mass range of 10 to 20 atomic mass units (amu) observed in CO_2 photodissociation at $h\nu$(VUV) = 11.832 eV (95,430.0 cm^{-1}) under different photoexcitation conditions. The top red trace shows the C^+ ion peak from $C(^3P_2)$ observed at 12 amu when both VUV_1 and VUV_2 were turned on in the interaction region. No C^+ ion was observed upon tuning of the VUV_2 laser off-resonance (black trace) or blocking of the VUV_1 beam in the interaction region (blue trace). The data thus clearly demonstrate that the observed C^+ ion intensity depends on both the VUV_1 photoexcitation of CO_2 and the VUV_2 photoionization of $C(^3P_2)$ photofragments. The ion peak at 18 amu, which was observed in all three mass spectra, is attributed to background H_2O^+ ions produced by VUV photoionization of ambient H_2O vapor in the photoionization chamber.

In Fig. 3, panels A to C compare the CO_2 photoabsorption spectrum reported by Archer *et al.* (*11*) to the photofragment excitation spectra obtained by detecting the $C(^3P_2)$ or the $O(^1S)$ fragments while tuning the VUV_1 over the energy range 11.562 to 12.212 eV (93,250 to 98,500 cm^{-1}). The photoabsorption spectrum of Fig. 3A shows the vibrational progressions of the $3p^1\Pi_u$ and 4s Rydberg states, which were identified previously by Cossart-Magos *et al.* (*12*) and Kuo *et al.* (*13*). The $C(^3P_2)$ and $O(^1S)$ photofragments were detected by VUV_2-visible (1+1') photoionization and VUV_2 excited autoionizing Rydberg state schemes with the excited $C^*[2s^22p3d\ (^3D^o{}_3)]$ and $O^*[2s^22p^3(^2P^o)3s\ (^1P^o{}_1)]$ Rydberg states, respectively, as VUV_2 resonant intermediate states. As shown in Fig. 3, A to C, the photofragment excitation spectra of $C(^3P_2)$ and $O(^1S)$ are in excellent agreement with the CO_2 photoabsorption spectrum, except that the 4s Rydberg peak of CO_2 at 11.967 eV (96,522 cm^{-1}) resolved in the spectrum of Fig. 3A is strongly perturbed or distorted in the $C(^3P_2)$ and $O(^1S)$ photofragment excitation spectra due to a strong dip in the VUV_1 tuning curve in this energy region. Because the $O(^1S) + CO(X^1\Sigma^+)$ channel is known to be a major nascent photoproduct channel in CO_2 photodissociation in this VUV energy range, the excellent agreement between the photofragment excitation spectra of $C(^3P_2)$ and $O(^1S)$ and the photoabsorption spectrum of CO_2 indicates that the $C(^3P_2)$ fragments are also nascent photoproducts in CO_2 photodissociation. The identification of $C(^3P_2)$ as a nascent photofragment clearly shows that the correlated O_2 photoproduct is formed in the VUV photodissociation of CO_2. The current photodissociation measurements on CO_2 were performed under molecular beam conditions to ensure that secondary collisions were unimportant. As pointed out above, the direct detection of $C(^3P_2)$ photofragments allows the measurement of the E_{int} distribution of the O_2 coincident photofragments using the VMI method. Because the photofragment excitation spectra of Fig. 3, B and C, have been normalized by the photodissociation VUV_1 laser intensity, which was monitored by measuring the photoionization efficiency spectrum of acetylene (C_2H_2) (*14*), the relative intensities of the $C(^3P_2)$ and $O(^1S)$ photofragment excitation spectra can be used to determine the relative yields of the $C(^3P_2) + O_2(X^3\Sigma_g^-)$ and $O(^1S) + CO(X^1\Sigma^+)$ photodissociation channels, respectively, in the CO_2 photodissociation energy range of $h\nu$(VUV) = 11.562 to 12.212 eV. Previous experimental studies suggest that the yield of the $O(^1S) + CO(X^1\Sigma^+)$ channel increases as the VUV photodissociation energy decreases (*15*), which is in good agreement with the CO_2 absorption spectrum and the observed $O(^1S)$ photofragment excitation spectrum of Fig. 3C. In comparison with the CO_2 absorption spectrum,

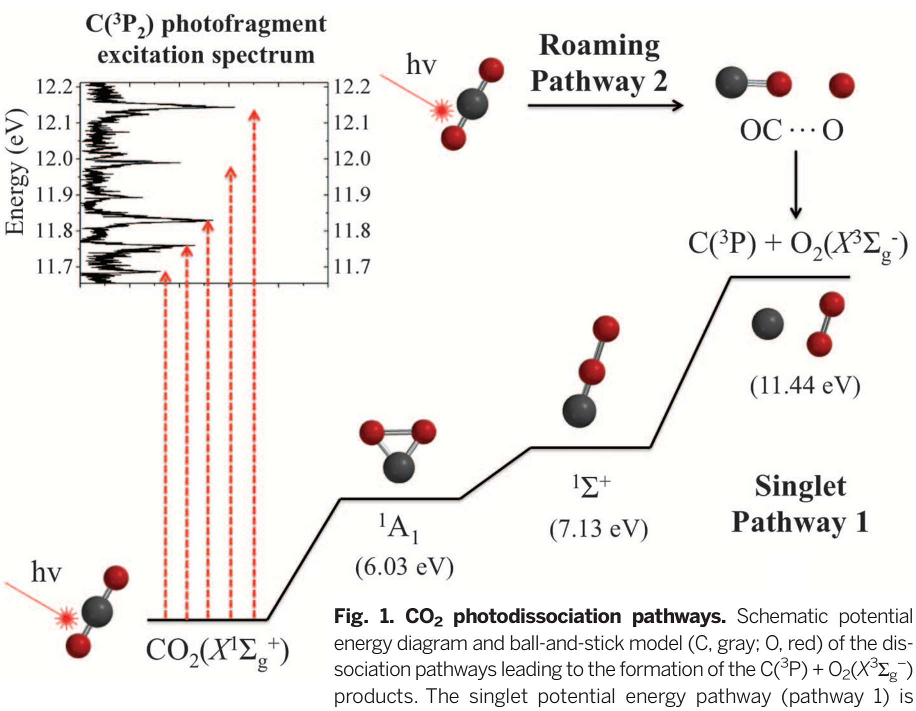

Fig. 1. CO_2 photodissociation pathways. Schematic potential energy diagram and ball-and-stick model (C, gray; O, red) of the dissociation pathways leading to the formation of the $C(^3P) + O_2(X^3\Sigma_g^-)$ products. The singlet potential energy pathway (pathway 1) is predicted to involve the formation of the c-$CO_2(^1A_1)$ and $COO(^1\Sigma^+)$ intermediates situated at 6.03 and 7.13 eV above the $CO_2(X^1\Sigma_g^+)$ ground state. Pathway 2 illustrates the roaming mechanism. The photoexcitation of a CO_2 molecule is indicated by the upward arrows to CO_2 absorption bands manifested by the $C(^3P_2)$ photofragment excitation spectrum in the energy range of 11.655 to 12.212 eV.

the observed $C(^3P_2)$ photofragment excitation spectrum of Fig. 3B shows that the yield of the $C(^3P_2) + O_2(X^3\Sigma_g^-)$ channel decreases as the VUV photodissociation energy decreases toward the thermochemical threshold for the formation of $C(^3P_2) + O_2(X^3\Sigma_g^-)$ at 11.44 eV. These observed dependences of the $C(^3P_2)$ and $O(^1S)$ intensities on the VUV photodissociation energy suggest that the branching ratio of the $C(^3P) + O_2(X^3\Sigma_g^-)$ channel relative to the $O(^1S) + CO(X^1\Sigma^+)$ channel is expected to increase as the VUV photodissociation energy increases. Based on the detection efficiencies for $C(^3P_2)$ and $O(^1S)$ in the present experiment and the measured $C(^3P_{2,1,0})$ fine structure distribution produced from CO_2 photodissociation, we have obtained an estimate of 5 ± 2% for the intensity of the $C(^3P) + O_2(X^3\Sigma_g^-)$ channel compared with that of the $O(^1S) + CO(X^1\Sigma^+)$ channel formed in CO_2 photodissociation in the current VUV photodissociation energy range near the energetic threshold of the $C(^3P) + O_2(X^3\Sigma_g^-)$ channel (*10*).

We have measured the $C(^3P_2)$ velocity-map ion images (Fig. 4) at five selected CO_2 predissociative states, as marked by the red downward pointing arrows in Fig. 3B. As shown below, the analysis of these $C(^3P_2)$ ion images provides further support for the direct formation of O_2 molecules in CO_2 photodissociation. The radial distribution of the $C(^3P_2)$ ion image (Fig. 4) provides a measure of the recoil velocity distribution of $C(^3P_2)$ photofragments produced at a specific VUV frequency for CO_2 excitation. The central donut-shaped ring structures of the $C(^3P_2)$ ion images originate from the formation of $C(^3P_2) + O_2(X^3\Sigma_g^-)$ in the photodissociation of CO_2. As the VUV_1 photon energy increases, the figures show that the radii of the ring structures observed for the $C(^3P_2)$ photofragments increase as expected. Based on the conservation of energy (Eq. 4) and linear momentum, the measurement of the $C(^3P_2)$ photofragments' recoil velocities can be used to determine the E_{trans} distribution of the O_2 counter-fragments and, thus, the TKER of the $C(^3P_2) + O_2(X^3\Sigma_g^-)$ product channel. The TKER spectra (Fig. 4, A to E) exhibit vibrational structures, from which we simulated the vibrational excitations of $O_2(X^3\Sigma_g^-)$ in the range of $v = 0$ to 3, as marked in the figures (*10*). The best fit to the observed vibrational profiles indicates that $O_2(X^3\Sigma_g^-)$ photofragments are also rotationally excited, with a rotational temperature well above 500 K. The onset energies of the TKER spectra are in excellent agreement with the thermochemical threshold (i.e., D_0 = 11.44 eV) for the formation of the $C(^3P_2) + O_2(X^3\Sigma_g)$ products from CO_2 photodissociation. The agreement of the $C(^3P_2) + O_2(X^3\Sigma_g^-)$ onset energies and the observation of the $O_2(X^3\Sigma_g^-)$ vibrational distributions are the most unambiguous evidence for the formation of the molecular oxygen channel in the VUV photodissociation of CO_2. Taking into account the theoretical results, we may rationalize that the production of molecular oxygen at photon energies near the energetic threshold proceeds mostly via the $c\text{-}CO_2(^1A_1)$ and $COO(^1\Sigma^+)$ intermediates on the singlet ground-state potential energy surface (pathway 1 in Fig. 1), which is predicted to have no potential energy barrier by the theoretical calculations (*7*, *8*).

The $C(^3P_2)$ ion image measurements reveal not only the E_{trans} distribution of the photoproduct channels, but also the angular distribution of the photofragments, which is characterized by the anisotropy β parameter (*16*). The angular distribution measurements provide information about the photodissociation rates for the formation of specific photofragments, as well as the geometry of the excited molecule at the time of its dissociation. The upper electronic states for the

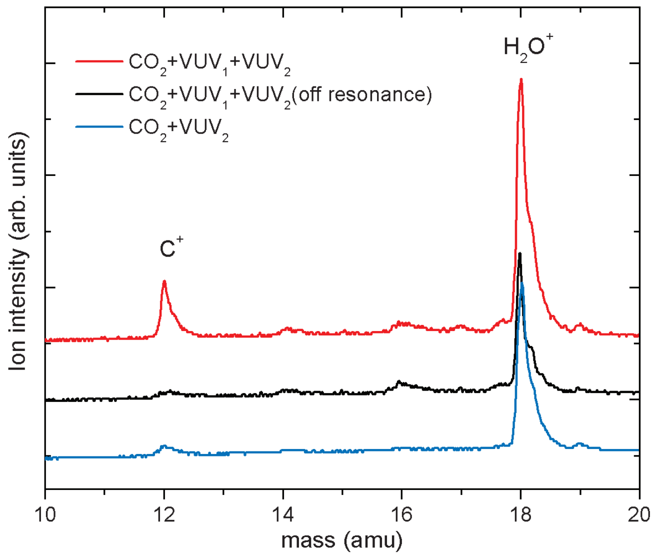

Fig. 2. Time-of-flight mass spectra from CO_2 photolysis at a VUV_1 energy of 11.832 eV (95,430.0 cm^{-1}). The top red trace indicates the detection of a C^+ ion from $C(^3P_2)$ with both VUV_1 and VUV_2 turned on. The black and blue traces below represent the background spectra observed by tuning the VUV_2 frequency off resonance and turning off the VUV_1 laser beam, respectively.

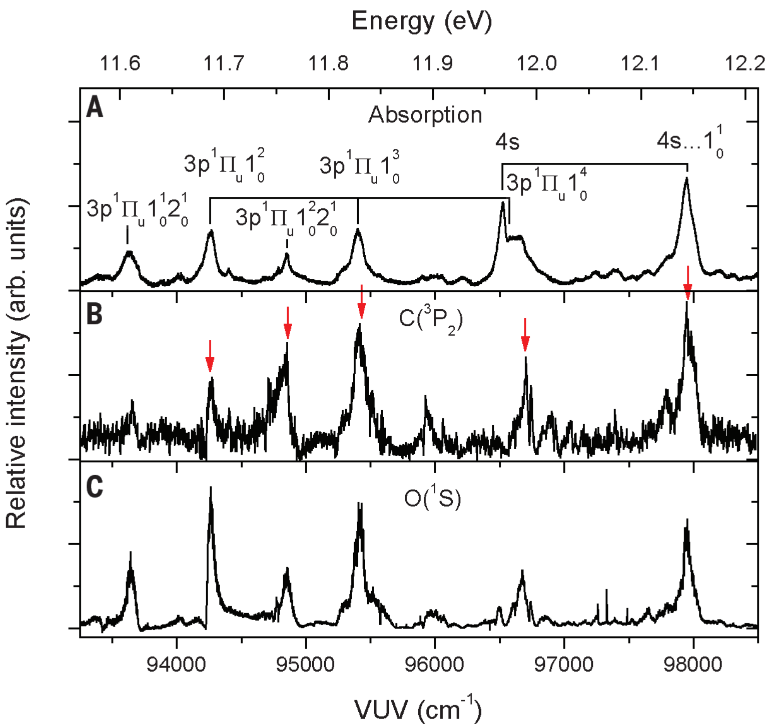

Fig. 3. Photofragment excitation spectra. Comparison of (**A**) the CO_2 absorption spectrum, (**B**) the photofragment excitation spectrum for $C(^3P_2)$, and (**C**) the photofragment excitation spectrum for $O(^1S)$ in the VUV_1 energy region 11.562 to 12.212 eV (93,250 to 98,500 cm^{-1}) illustrates that the $C(^3P_2)$ and $O(^1S)$ photofragments are observed only when CO_2 is photoexcited to an absorption band. The absorption spectrum was recorded by Archer *et al*. at an optical resolution of 1.15 cm^{-1} (full width at half maximum) (*11*). The red downward arrows mark the VUV_1 photodissociation energies at which $C(^3P_2)$ ion images were collected. The photofragment excitation spectra shown in (B) and (C) have been normalized by the corresponding VUV_1 laser intensity (*14*).

images in Fig. 4, A to C, are assigned as $3p^1\Pi_u$ (*12*, *13*). Thus, perpendicular distribution of the $C(^3P_2)$ atoms with respect to the CO_2 photolysis laser polarization is expected if CO_2 dissociates in a linear geometry. However, the $C(^3P_2)$ ion images reveal modest parallel distributions with respect to the transition dipole moment in Fig. 4, A to C. This result suggests that the electronically excited CO_2 molecules dissociate in a bent geometry for the formation of $C(^3P_2) + O_2(X^3\Sigma_g^-)$ products due to vibronic interaction. The parallel distribution of the photofragments has been observed in other triatomic molecules in perpendicular transitions due to vibronic interactions (*17*–*19*). The $3p^1\Pi_u$ Rydberg state of CO_2 is known to involve bending vibrational coupling (*20*), which is caused by the Fermi resonance between the excitation of one quantum of symmetric stretching (v_1) and two quanta of bending ($2v_2$) vibrational modes (*21*). Thus, the inclusion of vibronic interactions would account for the experimental observation of CO_2 dissociation in a bending geometry. The increase of the β value of 0.72 ± 0.07 in Fig. 4C to 0.97 ± 0.09 in Fig. 4D can be attributed to the symmetry change of the upper electronic states from $3p^1\Pi_u$ to 4s.

The recent experimental and theoretical evidence of a "roaming" dissociation pathway (*22*–*24*) has prompted us to speculate the involvement of O atom roaming for the formation of $C(^3P_2) + O_2(X^3\Sigma_g^-)$ products in CO_2 photodissociation (pathway 2 in Fig. 1). The roaming mechanism can be initiated via an incomplete OC-O bond cleavage. The resulting molecular CO and atomic O moieties interact via long-range forces on a flat region of the potential energy surface until they encounter a reactive site, leading to the formation of C + O_2 products by intramolecular O atom abstraction. Based on the theoretical calculation from Grebenshchikov (*8*), the CO_2 potential energy surfaces are relatively flat for the spin-allowed $CO(a^3\Pi) + O(^3P)$ and $CO(X^1\Sigma^+) + O(^1S)$ dissociation channels. The formation of $C(^3P_2) + O_2(X^3\Sigma_g^-)$ products can result from the O atom roaming with CO on these excited singlet surfaces in CO_2 photodissociation, similar to the roaming dissociation mechanism observed in NO_3 photodissociation (*24*).

Recently, Huestis *et al.* (*25*) suggested that the source of $O(^1S)$ day-glow emission observed from the Mariner 4 and Mars Express missions originates from the dissociative electron-ion recombination reaction (Eq. 5)

$$O_2^+ + e^- \rightarrow O_2^* \rightarrow O(^1S) + O(^3P) \qquad (5)$$

even though $O(^1S)$ atoms are known primary photofragments of VUV CO_2 photodissociation in the CO_2-dominated atmosphere of Mars. More recent measurements by Herschel spacecraft and Mars Science Laboratory's Sample Analyses at Mars provide O_2 abundance measurements of 1400 ± 120 parts per million (ppm) (*26*) and 1450 ± 90 ppm (*27*), respectively. The $O(^1S)$ optical emission poses an intriguing question about the source of O_2^+, which can be produced by VUV photoionization of O_2 and/or charge transfer from CO_2^+ to O_2 in the CO_2-dominated atmosphere of Mars. Our study has provided unambiguous experimental evidence for the formation of C + O_2 photoproducts in CO_2 photodissociation. We suggest that this pathway for generating O_2 be incorporated into future photochemical reaction networks and general circulation models of planetary atmospheres dominated by CO_2.

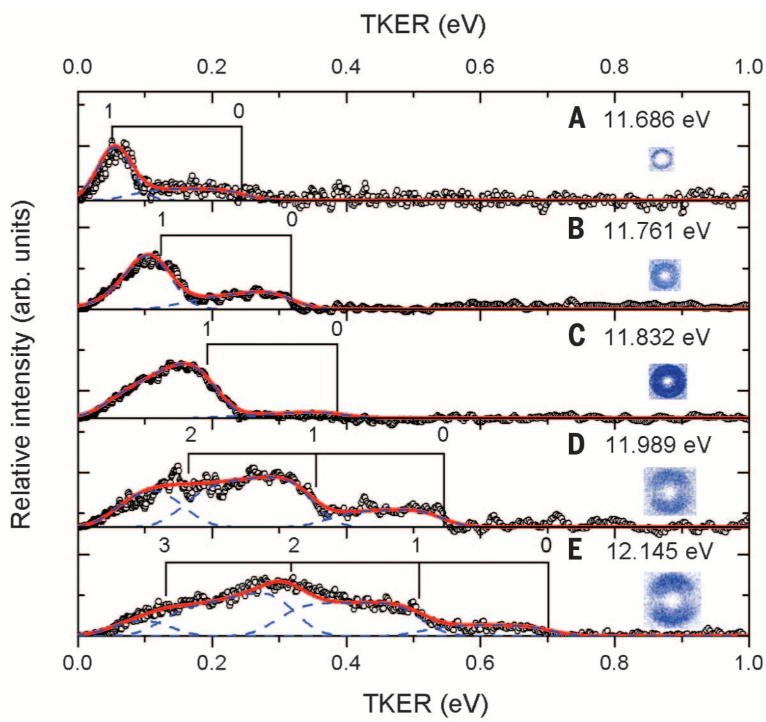

Fig. 4. $C(^3P_2)$ velocity-map ion images and corresponding TKER spectra. VUV_1 photoexcitation of CO_2 was tuned to the absorption bands peaked at the energies indicated above the ion image inserts. TKER spectra are plotted as open circles. Angular anisotropy β parameters derived from these $C(^3P_2)$ ion images are (**A**) β = 0.45 ± 0.09, (**B**) β = 0.45 ± 0.08, (**C**) β = 0.72 ± 0.07, (**D**) β = 0.97 ± 0.09, and (**E**) β = 1.02 ± 0.08. The simulation (red lines) shows that the threshold energies observed are consistent with the known thermochemical threshold of 11.44 eV for the $C(^3P) + O_2(X^3\Sigma_g^-)$ channel, and $O_2(X^3\Sigma_g^-)$ photofragments are formed in v = 0 to 3 vibrational levels, as marked on top of the TKER spectra of (A) to (E). The dashed lines show the simulated rotational profiles of individual vibrational bands of $O_2(X^3\Sigma_g^-)$.

REFERENCES AND NOTES

1. H. D. Holland, *Philos. Trans. R. Soc. London Ser. B* **361**, 903–915 (2006).
2. H. D. Holland, *Geochim. Cosmochim. Acta* **73**, 5241–5255 (2009).
3. J. W. Schopf, *Annu. Rev. Earth Planet. Sci.* **3**, 213–249 (1975).
4. J. F. Kasting, S. Liu, T. Donahue, *J. Geophys. Res.* **84**, 3097–3107 (1979).
5. J. F. Kasting, J. C. Walker, *J. Geophys. Res.* **86**, 1147–1158 (1981).
6. J. F. Kasting, J. B. Pollack, D. Crisp, *J. Atmos. Chem.* **1**, 403–428 (1984).
7. D. Y. Hwang, A. M. Mebel, *Chem. Phys.* **256**, 169–176 (2000).
8. S. Y. Grebenshchikov, *J. Chem. Phys.* **138**, 224106 (2013).
9. H. Gao, Y. Song, W. M. Jackson, C. Y. Ng, *J. Chem. Phys.* **138**, 191102 (2013).
10. Materials and methods are detailed in the supplementary materials on *Science* Online.
11. L. Archer *et al*., *J. Quant. Spectrosc. Radiat. Transf.* **117**, 88–92 (2013).
12. C. Cossart-Magos, M. Jungen, F. Launay, *Mol. Phys.* **61**, 1077–1117 (1987).
13. C. T. Kuo, Y. M. Chen, S. Y. Wang, S. C. Li, J. B. Nee, *Chin. J. Physiol.* **42**, 65–73 (2004).
14. V. H. Dibeler, J. A. Walker, *Int. J. Mass Spectrom. Ion Phys.* **11**, 49–56 (1973).
15. G. M. Lawrence, *J. Chem. Phys.* **57**, 5616–5617 (1972).
16. D. W. Chandler, P. L. Houston, *J. Chem. Phys.* **87**, 1445–1447 (1987).
17. S. H. Kable *et al*., *J. Phys. Chem.* **95**, 8013–8018 (1991).
18. J. Riedel, S. Dziarzhytski, A. Kuczmann, F. Renth, F. Temps, *Chem. Phys. Lett.* **414**, 473–478 (2005).
19. J. i. Adachi, N. Kosugi, E. Shigemasa, A. Yagishita, *J. Chem. Phys.* **107**, 4919–4926 (1997).
20. H. J. Werner, A. Spielfiedel, N. Feautrier, G. Chambaud, P. Rosmus, *Chem. Phys. Lett.* **175**, 203–208 (1990).
21. M. A. Gharaibeh, D. J. Clouthier, *J. Chem. Phys.* **132**, 114307 (2010).
22. D. Townsend *et al*., *Science* **306**, 1158–1161 (2004).
23. A. G. Suits, *Acc. Chem. Res.* **41**, 873–881 (2008).
24. M. P. Grubb *et al*., *Science* **335**, 1075–1078 (2012).
25. D. L. Huestis, T. G. Slanger, B. D. Sharpee, J. L. Fox, *Faraday Discuss.* **147**, 307–322 (2010).
26. P. Hartogh *et al*., *Astron. Astrophys.* **521**, L49 (2010).
27. P. R. Mahaffy *et al*., *Science* **341**, 263–266 (2013).

ACKNOWLEDGMENTS

This work was supported in part by NASA Origins of Solar Systems Program grant no. NNX13AJ50G and an Institute of Geophysics and Planetary Physics–Los Alamos National Laboratory University of California grant to Q.-Z.Y. and C.Y.N. Additionally, C.Y.N. was supported by U.S. Department of Energy contract no. DE-FG02-02ER15306. W.M.J. was supported NSF grant no. CHE-1301501. We thank S. Y. Grebenshchikov at the Technical University of Munich for discussions and G. Stark for providing the digitized CO_2 photoabsorption spectrum.

SUPPLEMENTARY MATERIALS

www.sciencemag.org/content/346/6205/61/suppl/DC1
Materials and Methods
Figs. S1 to S4
References (*28*–*37*)

9 June 2014; accepted 19 August 2014
10.1126/science.1257156